The Thermal Evolution of Mars Modulated by Mantle Melting

Abigail Ann Fraeman

Advisor: Jun Korenaga
2nd Reader: David Bercovici
April 29, 2009

A Senior Thesis presented to the faculty of the Department of Geology and Geophysics, Yale University, in partial fulfillment of the Bachelor's Degree.

Abstract

Melting in the mantle during convection leads to the formation of a compositionally buoyant lithosphere, which may also be intrinsically more viscous by dehydration. The consequences of these melting effects on the evolution of terrestrial planets have not been explored before. In this study, we incorporate a new heat-flow scaling law for stagnant lid convection into a parameterized convection model of Mars to better understand how its thermal evolution may be affected by mantle melting. The temporal evolution of crust and mantle lithosphere is modeled in a self-consistent manner considering mantle melting, convective instability, and potential rewetting of dehydrated lithosphere from below by hydrogen diffusion. Overall, our models show the effects of compositional buoyancy on Mars' cooling history is minimal. The introduction of viscosity contrast between wet and dry mantle, however, can modify the thermal evolution substantially. Higher viscosity contrasts result in lower crustal thickness, higher mantle temperatures, and lower surface and core heat fluxes. Additionally, our models predict a much greater degree of dehydration in the mantle than previously suggested, and the loss of such a large amount of water from the mantle to surface has significant implications about the role of water in the early surface and climate evolution of Mars.

1. Introduction

The thermal evolution of a terrestrial planet has a significant impact on the planet's tectonic, magnetic, and geologic history. These wide ranging effects have motivated a large number of studies that attempt to reconstruct the cooling histories of terrestrial planets [e.g. *Stevenson et al.*, 1983, *Hauck and Phillips* 2002].

The effects of mantle melting may have a significant impact on the thermal evolution of terrestrial planets because mantle melting introduces compositional and viscosity stratifications in the shallow mantle [*Korenaga*, Submitted]. Compositional stratifications occur when mantle melting preferentially removes incompatible elements, creating a depleted boundary layer that is less dense then the primitive mantle. This depleted layer generates a layer of positive buoyancy that offsets the negative thermal buoyancy of the cooling of thermal boundary layer. The conflict between positive compositional and negative thermal buoyancy can cause the depleted layer to become unstable and undergo alternating periods of accumulation and delamination over a substantial portion of the planet's evolution [*Parmentier and Hess*, 1992].

Viscosity stratifications will be present due to the difference in water content between the primitive and melted mantle. Hydrogen is a highly incompatible element, so an upwelling mantle becomes almost completely dehydrated at the onset of melting [*Hirth and Kohlstedt*, 1996]. The viscosity differences between wet and dry mantle are significant, and may be on the order of $10^2 - 10^3$ for dislocation creep scenarios [*Hirth and Kohlstedt*, 1996; *Korenaga and Karato*, 2008] and ~10 for diffusion creep [*Korenaga and Karato*, 2008]. These viscosity variations create a stiff dehydrated lid that reduces surface heat flux [*Korenaga*, Submitted].

Korenaga [submitted] has taken the effects of compositional and viscosity stratification into consideration in deriving a new heat-flow scaling law for stagnant lid convection. For Earth, this new scaling law reverts the sense of heat-flow scaling for the internal Rayleigh number (Ra_i), which makes the surface heat flux relatively insensitive to the change in mantle temperature. In Mars and other small terrestrial planets, the effects of mantle melting on heat-flow scaling becomes visible at lower temperature than Earth due to the lower gravity of Mars.

Overall, *Korenaga* [submitted] concluded the mantle melting could reduce the conventional prediction of surface heat flux by up to a factor of ~5-10.

In this study, we apply the stagnant-lid convection model of *Korenaga* [submitted] to a parameterized cooling model of Mars in order to understand the full effects of these new scaling laws. The consequences of mantle melting are thought to be the most significant for small terrestrial planets like Mars because the initial pressure of melting occurs at greater depths in these small planets [*Korenaga*, Submitted; *Takahashi and Kushiro*, 1983]. Mars also likely had a wet mantle [*Lunine et al.*, 2003; *Wanke and Dreibus*, 1994], so the effects of viscosity stratification caused by dehydration stiffening should be relevant Mars. Finally, the low pressures on Mars mean that the Martian mantle acts in a similar fashion to the well-characterized upper mantle of the Earth.

2.0 Methods

We have generated a parameterized convection-cooling model to monitor the thermal evolution of Mars. We have recreated the calculations described in *Stevenson et al.*, [1983] to model core cooling and inner core formation, and the techniques of *Hauck and Phillips* [2002] to account for a coupled crustal-magmatic evolution. We have added new parameters to track the chemical evolution of the mantle lithosphere and convection mantle, and incorporated a new heat-flow scaling law that takes into account mantle melting effects [*Korenaga*, Submitted]. Finally, we have included variables to model the effects of rewetting of the dehydrated lithosphere from hydrogen diffusion and mass transport by convective instabilities.

2.1 Parameterized Model Overview and Governing Equations

A parameterized cooling model can be used to monitor the changes in mantle temperature over time [*Stevenson et al.*, 1983]. This model assumes the mantle is a spherical shell overlying a concentric spherical core. Both the core and mantle have constant densities, ϱ_c and ϱ_m, and whole mantle convection is assumed, consistent with Stevenson et al, 1983.

The change in mantle (T_u) and core (T_c) temperatures over time are determined by solving for the equations of energy conservation; that is the time rate of change of the thermal energy must be equal to the difference between the rate of radioactive heat production and the radioactive heat transfer across the thermal boundary layer.

Equation (1) is the differential equation for conservation of energy in the mantle and may be used to solve for the change in T_u over time:

$$\frac{4}{3}\pi\left(R_p^3 - R_c^3\right)\left\{Q_{mantle} - \rho_m C_m \eta_m \frac{dT_u}{dt}\right\} - \rho_m f_{pm} L_{pm} = 4\pi\left(q_m R_p^2 - F_c R_c^2\right)$$

<div align="right">**Equation 1**</div>

R_p is the radius of the planet, R_c is the radius of the core, η_m is a constant relating upper mantle temperature to average mantle temperature, and ϱ_m and C_m are the density and heat capacity of the mantle. Q_{mantle} is the heat production per unit volume in the mantle, f_{pm} is the volumetric melt production, and L_{pm} is the latent heat released during melting. F_c and q_m are the heat fluxes at the core and mantle/crustal boundary respectively. Q_{mantle}, f_{pm}, F_c, and q_m all vary with time and must be calculated in the model.

Isolating dTu/dt to one side gives us:

$$\frac{dT_u}{dt} = \left(\frac{4\pi\left\{ q_m R_p^2 - F_c R_c^2 \right\} + \rho_m f_{pm} L_{pm}}{\frac{4}{3}\pi\left(R_p^3 - R_c^3 \right)} - Q_{mantle} \right)\left(-\rho_m C_m \eta_m \right)^{-1}$$

We also want to solve for the change in temperature at the core mantle boundary over time using

$$\left\{ (L + E_G)4\pi R_i^2 \rho_c \frac{dR_i}{dT_{cm}} - \frac{4}{3}\pi R_c^3 \rho_c C_c \eta_c \right\} \frac{dT_{cm}}{dt} = 4\pi R_c^2 F_c$$

where R_i is the radius of the inner core, T_{cm} is the temperature at the core-mantle boundary, η_c is a constant, and ϱ_c and C_c are the core density and heat capacity. L and E_G are constants to account for the energy released with the formation of an inner core; L is the latent heat of solidification and E_G is the gravitational energy made available per unit mass of inner core material. dR_i/dT_{cm} also varies with time, and must be calculated.

Rearranging we find that

$$\frac{dT_{cm}}{dt} = 4\pi R_c^2 F_c \left\{ (L + E_G)4\pi R_i^2 \rho_c \frac{dR_i}{dT_{cm}} - \frac{4}{3}\pi R_c^3 \rho_c C_c \eta_c \right\}^{-1}$$

2.2 Calculating Inner Core Growth

We keep track of inner core growth in order to find dR_i/dT_{cm} and solve Equation (4). We begin by calculating the liquidus temperature in the core to determine if any inner core growth has occurred. First, we need to find the mass fraction of light alloying constituents in the core. This is given by:

$$x = \frac{x_0 R_c^3}{R_c^3 - R_i^3}$$

<div align="right">**Equation 5**</div>

where x_0 is the initial concentration of light constituents in the core. This value is not known for Mars, and may range between 0.1 and 0.25 [*Stevenson et al.*, 1983].

The inner core will only begin to grow when the temperature at the core mantle boundary is below the critical liquidus temperature. To determine this we first calculate the liquidus temperature at the center of the planet

$$Tm_c = Tm_0(1 - \alpha_c x)(1 + Tm_1 P_c + Tm_2 P_c^2)$$

<div align="right">**Equation 6**</div>

where Tm_0, Tm_1, Tm_2 and α_c are constants. P_c is the pressure at the center of the planet.

We then use the equation for the adiabat to determine the critical core temperature at the core mantle boundary

$$T_{cmCrit} = Tm_c \left\{ \frac{1 + T_{a1} P_{cm} + T_{a2} P_{cm}^2}{1 + T_{a1} P_c + T_{a2} P_c^2} \right\}$$

<div align="right">**Equation 7**</div>

where T_{a1} and T_{a2} are constants, and P_{cm} is the pressure at the core-mantle boundary. If T_{cm} is not less than T_{cmCrit} there is no inner core formation and the pressure at the inner/outer core boundary, P_{io}, equals the pressure at the center of the planet and the inner core radius, and dR_i/dT_{cm} equal 0.

If our value for T_{cm} is less than the T_{cmCrit} value, we expect an inner core to form. In this case, we need calculate the pressure at the inner-outer core boundary, the radius of the inner

core, and the change in inner core radius over change in T_{cm}. First, we'll find P_{io}. We can find the liquidus temperature of the core alloy as a quadratic function of pressure:

$$T_m(r) = T_{m0}(1 - \alpha_c x)(1 + T_{m1}P(r) + T_{m2}P^2(r))$$

The parameter choices above are related to the parameters that enter the core adiabat, which is:

$$T_c(r) = T_{cm}\left\{\frac{1 + T_{a1}P(r) + T_{a2}P^2(r)}{1 + T_{a1}P_{cm} + T_{a2}P_{cm}^2}\right\}$$

When the temperature of the outer core is equal to the temperature of the mantle we can set equations (8 and 9) equal to each other and solve for the pressure at the mantle/core boundary, P_{i0}:

$$T_{m0}(1 - \alpha_c x)(1 + T_{m1}P(r) + T_{m2}P^2(r)) = T_{cm}\left\{\frac{1 + T_{a1}P(r) + T_{a2}P^2(r)}{1 + T_{a1}P_{cm} + T_{a2}P_{cm}^2}\right\}$$

This reduces to:

$$P(r) = \frac{-(aT_{m1} - T_{a1}) \pm \sqrt{(aT_{m1} - T_{a1})^2 - 4(aT_{m2} - T_{a2})(a - 1)}}{2(aT_{m2} - T_{a2})} = P_{io}$$

where

$$a = \frac{T_{m0}(1 - \alpha_c x)}{T_{cm}}(1 + T_{a1}P_{cm} + T_{a2}P_{cm}^2)$$

Now that we know the pressure at inner/outer core boundary (P_{i0}), we can calculate the radius of the inner core as

$$R_i = \sqrt{\frac{2(P_c - P_{io})R_c}{\rho_c g}}$$

We need to calculate dR_i/dT_{cm} to use in equation (4). The chain rule makes the problem easier to solve:

$$\frac{dR_i}{dT_{cm}} = \frac{dR_i}{dP_{io}} \frac{dP_{io}}{dT_{cm}}$$

We find:

$$\frac{dR_i}{dP_{io}} = \frac{d}{dP_{io}} \sqrt{\frac{2(P_c - P_{io})R_c}{\rho_c g}} = -\frac{R_c}{\sqrt{2R_c \rho_c g(P_c - P_{io})}}$$

and

$$\frac{dP_{io}}{dT_{cm}} = \frac{T_{cm} + 1 + T_{a1}P_{io} + T_{a2}P_{io}^{\ 2} - A}{AT_{m1} + AT_{m2}2P_{io} - T_{cm}T_{a1} - T_{cm}T_{a2}2P_{io}}$$

where

$$A = Tm_0(1 - \alpha_c x)(1 + T_{a1}P_{cm} + T_{a2}P_{cm}^{\ 2})$$

2.3 Mantle Melting

We have modified the methods of *Hauck and Phillips* [2002] to calculate melt production and crust formation, described below.

2.3.1 Melt production rate

Melting in a stagnant lid, convecting system occurs predominantly due to the adiabatic decompression of passively upwelling material [*Hauck and Phillips*, 2002]. The initial pressure of melting occurs when the temperature of mantle material crosses the solidus at

$$P_{initial} = \frac{T_u - 1150}{\left(120 \cdot 10^{-9}\right) - \dfrac{dT}{dP}}$$

where T_u is in units of Kelvin and dT/dP is the adiabatic gradient equal to 1.54e-8 K/Pa. Melting ceases at the base of the stagnant lid when the pressure is equal to

$$P_{final} = \rho_m \cdot g \cdot \left(z + h_c\right)$$

where h_c is the thickness of the crust and z is the thickness of the thermal boundary layer calculated by

$$z = \frac{d}{Nu}$$

Nu is the Nusslet number and d is the mantle depth. The initial and final depths of melting are

$$z_0 = \frac{P_{initial}}{\rho_m \cdot g}$$

$$z_f = \frac{P_{final}}{\rho_m \cdot g}$$

If the initial pressure of melting is greater than the final pressure, the mantle is melting and the melt fraction is

$$\phi = \frac{\left(P_{initial} - P_{final}\right)}{2} \cdot \frac{dF}{dP}$$

where dF/dP is the change in melt fraction with the change in pressure above the solidus equal to 0.12e-9.

To calculate the volumetric melt production, we assume the upwelling mantle is approximately cylindrical and calculate the flux of material through the melt-channel [*Reese et al.*, 1998]. Figure 1 is an illustration of the cylindrical mantle differentiation model. We take the radius of the cylinder to be equal to the mantle depth, d, because convection typically takes an aspect ratio of one-to-one. In stagnant-lid convection, downwelling material tends to be much more focused than upwelling material, so we can also make the assumption that all downwelling occurs at the edge of the cylinder.

The flux of mantle leaving the melting zone is

$$\Phi_{mantle} = \left(2\pi d\right) \cdot z_m \cdot u_i$$

where u_i is the convecting velocity of the mantle calculated as described in section 2.3.2 and $z_m = z_0 - z_f$. The total melt flux for the cylinder is equal to the mantle flux times the melt fraction

$$\Phi_{melt} = \left(2\pi d\right) \cdot z_m \cdot u_i \cdot \phi$$

The total surface area of a cylinder is $SA = \pi d^2$, so the melt productivity per unit area is

$$\Phi_{melt/unit\ area} = \frac{\Phi_{melt}}{\pi d^2} = \frac{2z_m u_i \phi}{d}$$

Finally, we multiply this by the surface area of the planet to get the whole-planet melt productivity

$$f_{pm} = \frac{2z_m u_i \phi}{d} \cdot 4\pi R_p^2$$

2.3.2 Viscosity and convecting velocity

In a time-dependent regime, the equation of the convecting velocity is [*Solomatov and Moresi*, 2000]

$$u_i = \frac{\kappa}{d}\left(0.04 + 0.34n^{-1}\right)\left(\frac{Ra_i}{\theta}\right)^{\frac{n(2n+1)}{(n+1)(n+2)}}$$

where κ is a the mantle thermal diffusivity and n is the exponential dependence of viscosity on stress. n has a value of one for Newtonian-flow and values greater than one for non-Newtonian flows.

Ra_i is the internal Rayleigh number, a dimensionless value that determines the nature of heat transfer in the system. Ra_i is calculated by

$$Ra_i = \frac{\alpha \rho_m g \Delta T d^{(n+2)/n}}{\kappa^{1/n} \eta_i^{1/n}}$$

where α is the mantle thermal expansivity, ΔT is the temperature drop across the layer, and η_i is the mantle viscosity.

We modify this equation from that provided in *Hauck and Phillips* [2002] in order to take into account the viscosity changes that will occur as the mantle dehydrates. We use exponential form of the viscosity equation and calculate η_i as a function of temperature and water content in the mantle.

$$\eta_i = c \cdot \exp\left(\frac{E}{RT_u}\right) \cdot \Delta\eta^{1-C_H^{cm}}$$

In this equation, c is a viscosity constant. The viscosity contrast between the wet and dry mantle is represented by $\Delta\eta$, which may range in values from 10-10^3 [*Korenaga and Karato*, 2008] and C_H^{cm} is normalized value representing the water concentration in the convecting mantle. C_H^{cm} has an initial value of one and decreases as the mantle dehydrates.

θ is the Frank-Kamenetiskii approximation and describes the natural logarithm of the viscosity contrast across the mantle.

$$\theta = \ln(\Delta\eta) = \frac{E}{RT_u^2}\Delta T$$

E is the activation energy and R is universal gas constant. The model experiences problems when θ becomes too small. When this occurs, system enters an isoviscous regime where viscosity does not change with temperature and conventional heat-flow scaling laws do not apply. To avoid this problem, we chose a value $\theta_{min}=1.2(n+1)$, and set $\theta=\theta_{min}$ whenever $\theta<\theta_{min}$.

2.3.3 Mass transport of incompatible elements by mantle melting

The convecting mantle will become depleted in incompatible elements over time, while the crust and lithosphere will become enriched with them. We therefore need to keep track of the volume of the mantle that has been melted in order to determine the changing concentrations of incompatible elements in the convecting mantle and the crust/lithosphere. The equation for the fractionation of these incompatible elements due to a batch-melting model is given by

$$C_{melt} = C_{mantle} \frac{1}{\phi + D(1 - \phi)}$$

where C_{melt} and C_{mantle} are the concentrations of incompatible elements in the melt and mantle, ϕ is the volume fraction of the melt, and D is the bulk distribution coefficient.

Hauck and Phillips [2002] report using a value of D=0.1 for heat producing elements in their model of crust formation. However, the value of D for Hydrogen in olivine/melt is around 0.002 ± 0.0002 [*Koga et al*., 2003] and 0.01 for Thorium and Uranium in clinopyroxene/melt [*Hauri et al*., 1994]. These values are closer to zero than to 0.1, so we therefore make the approximation of $D = 0$ both for water and heat producing elements.

For simplicity, we assume that all melt is extracted to form crust. After each time step in the model, the increase in volume of the crust is equal to

$$\Delta V_{crust} = f_{pm} \cdot dt$$

where dt is the timestep. The change in volume of the depleted mantle lithosphere is

$$\Delta V_{dml} = f_{pm} \cdot \frac{1 - \phi}{\phi} \cdot dt$$

The amount of mantle that has been processed in each timestep is equal to

$$\Delta V_{processed} = -\Delta V_{convecting} = \frac{f_{pm}}{\phi} \cdot dt$$

The amount of heat that would be produced in a non-convecting, primitive mantle as a function of time is

$$W_{pm} = \left(Q_0 e^{-\lambda t}\right) V_{pm}$$

where V_{pm} is the volume of the primitive mantle, Q_0 is the initial heat source density, and lambda is the radioactive decay constant. The fraction of this initial heat that is sequestered to the crust is

$$W_{crust} = W_{crust\_old} e^{-\lambda dt} + Q_{cm} \cdot \Delta V_{processed} \cdot \frac{1}{\phi + D(1 - \phi)}$$

Q_{cm} is the heat density in the convecting mantle, calculated by

$$Q_{cm} = \frac{W_{pm} - W_{crust}}{V_{mantle}}$$

We also want to keep track of the amount of water that has left the mantle due to dehydration during melting. A "normalized", dimensionless quantity C_H^{cm} is used to represent the fraction of water remaining in the mantle. After each time step,

$$H_{surface} = H_{surface\_old} + C_H^{cm} \cdot \Delta V_{processed} \cdot \frac{1}{\phi + D(1 - \phi)}$$

where $H_{surface}$ represents the volume of water brought to the surface. Since dehydrated water leaves the mantle, the amount of water in the convecting mantle decreases by

$$H_{cm} = H_{pm} - H_{surface}$$

where H_{pm} is the volume of water in the primitive mantle equal to the product of the normalized value C_H^{cm} and the volume of primitive mantle. We update the value of C_H^{cm} to reflect the present volume of water in the convecting mantle by using

$$C_H^{cm} = \frac{H_{cm}}{V_{mantle}}$$

Finally, we are able to calculate the new crustal and depleted mantle lithospheric thicknesses as

$$h_c = R_p - \left(R_p^3 - \frac{3V_{crust}}{4\pi} \right)^{1/3}$$

$$h_l = \left(R_p - h_c \right) - \left(\left(R_p - h_c \right)^3 - \frac{3V_{dml}}{4\pi} \right)^{1/3}$$

2.4 Calculating Nu number

We calculate the Nusselt using the method described in *Korenaga* [Submitted]. This method calculates Nu as a number with temperature-dependent viscosity based on the local stability criterion. In our model, $Nu = F_{Nu} (Ra_i, n, \theta, E, \Delta T, T_S, h_C, \Delta\eta, \Delta\varrho)$.

16

2.5 Calculating core and surface heat flux

2.5.1 Core heat flux

We use the method of *Stevenson et al.*, [1983] to calculate core heat flux, which is given by the equation

$$F_c = \frac{k(T_{cm} - T_l)}{\delta}$$

<div align="right">**Equation 44**</div>

k is the mantle thermal conductivity, T_{cm} is the temperature of the core-mantle boundary, T_l is the temperature of the lower mantle, and δ is the boundary layer thickness.

The value of T_l may be found using the equation

$$T_l = T_u + \frac{dT}{dr}(R_p - R_c)$$

<div align="right">**Equation 45**</div>

Where

$$\frac{dT}{dr} = \frac{\alpha g T}{C_p}$$

<div align="right">**Equation 46**</div>

Since temperature changes with depth, we can use the average adiabatic gradient and $<T_m>$, the average mantle temperature. In this case, our equation for T_l becomes

$$T_l = T_u + f <T_m>$$

<div align="right">**Equation 47**</div>

Where 'f' is a constant, which can be determined as follows:

$<T_m>$ is the weighted average of T_u and T_l so we can express it as:

$$< T_m >= aT_u + (1-a)T_l = aT_u + (1-a)(T_u + f < T_m >) = \frac{1}{1-(1-a)f}T_u$$

We also know that

$$< T_m >= \eta_m T_u$$

So

$$\eta_m = \frac{1}{1-(1-a)f}$$

$$f = \frac{\eta_m - 1}{(1-a)\eta_m}$$

We know all of these values except for 'a', which is another constant found by

integrating the equation

$$< T_m >= \frac{4\pi}{\frac{4}{3}\pi(R_p^3 - R_c^3)} \int_{R_c}^{R_p} r^2 T_m(r)dr$$

Where

$$T_m(r) = T_l + (T_u - T_l)\frac{r - R_c}{R_p - R_c}$$

The result of the integration will be in the form $<T_m> = bT_l + aT_u$ where a+b=1.

There are two methods for determining the value of δ, and we choose the method that generates the smaller value. In the first method, the equation for delta is given by

$$\delta = \left(R_p - R_c\right)\left(\frac{Ra_{cr}}{Ra}\right)^{\beta}$$

Where β and Ra_{cr} are constants. Ra is the Rayleigh number defined as

$$Ra \equiv \frac{g\alpha((T_u - T_s) + (T_{cm} - T_l))(R_p - R_c)^3}{\nu K}$$

ν is the kinematic viscosity of the mantle and is related to absolute upper mantle temperature by:

$$\nu = \nu_0 e^{A/T_u}$$

In the second method we want to find the local critical Rayleigh number for the breakdown of the boundary layer given by

$$Ra_{crb} = \frac{g\alpha(T_{cm} - T_u)\delta_c^3}{\nu_c K}$$

We isolate delta and get the equation

$$\delta_c = \left[\frac{(Ra_{crb})(\nu_c K)}{g\alpha(T_{cm} - T_u)}\right]^{1/3}$$

We know or have calculated all of the values in this equation except ν_c which we find using

$$v_c = v_0 e^{A/T_l + \frac{T_u - T_{cm}}{2}}$$

2.5.2 Surface heat flux

Our method for finding surface heat flux differs from that of *Stevenson et al*., [1983] due to fact that heat-producing elements are sequestered in the crust. These elements generate a significant amount of heat close to the surface that needs to be taken into account in calculating surface heat flux.

Incompatible, heat-producing elements are placed in the crust an exponential, rather than linear, distribution. Two main reasons support this choice of distribution:

1) Crust on Mars is similar to oceanic, rather than continental, crust on Earth. While the distribution of heat producing elements in continental crust is still debated, experimental evidence of Mars-like oceanic crust has suggested that heat-producing elements are preferentially distributed at the top of oceanic crust [*Lachenbruch*, 1970]. Using an exponential distribution is one way to approximate the layered nature of heat producing elements.

2) The results from running our model with exponential distribution are more reasonable than with a linear distribution

To create the exponential distribution we follow the method of *Turcotte and Schubert* [2002]. Assume that heat production due to radioactive elements decreases exponentially with depth in the following manner:

$$H = H_s e^{\frac{-z}{h_r}}$$

Where H_s is the surface (z=0) radiogenic heat production rate per unit mass, and h_r is a length scale for the decrease in H with depth. $h_r = h_c/4$ in this model.

The equation for energy conservation is

$$0 = k\frac{d^2T}{dz^2} + \rho H$$

We substitute the equation for H into the equation for energy conservation and get

$$0 = k\frac{d^2T}{dz^2} + \rho H_s e^{-\frac{z}{h_r}}$$

Integrating this equation produces

$$c_1 = k\frac{dT}{dz} - \rho H_s h_r e^{-\frac{z}{h_r}}$$

Integrating it again produces

$$c_1 z + c_2 = k\frac{dT}{dz} + \rho H_s h_r^2 e^{-\frac{z}{h_r}}$$

When z =0

$$c_2 = kT_s + \rho H_s h_r^2$$

By definition we know

$$q(z) = k\frac{dT}{dz} = c_1 + \rho H_s h_r e^{-\frac{z}{h_r}}$$

We know also q(h) = q$_m$ where h is the crustal thickness, so

$$c_1 = q_m - \rho H_s h_r e^{-\frac{h}{h_r}}$$

We can say

$$T_c = T(h) = \frac{c_1 h + c_2 - \rho H_s h_r^2 e^{-\frac{h}{h_r}}}{k}$$

Now we plug in the values we calculated for c_1 and c_2. Finally, we need to solve for H$_s$.

$$\int_0^h H_s e^{-z/h_r} dz = H_s h_r (1 - e^{-h/h_r})$$

So

$$H_s = \frac{H_0 h}{h_r (1 - e^{-h/h_r})}$$

The heat flux at the base of the crust is calculated as

$$q_m = Nu\frac{K(T_u - T_c)}{d}$$

and the surface heat flux is

$$Fs = qm + \rho_m Hh_c$$

2.6 Rewetting from Below by Hydrogen Diffusion

Unmelted (wet) mantle continuously re-hydrates the bottom-most layer of dehydrated lithosphere by hydrogen diffusion [*Korenaga*, Submitted].   We consider the effects of this rehydration in our thermal evolution model because they have the potential to undermine the significance of dehydration stiffening.

Korenaga [Submitted] demonstrates that, assuming the mantle has not been completely dehydrated, the dimensionalized diffusion distance of hydrogen may be represented as

$$d \approx \left(D_{H,eff}^* D_{H,0} t\right)^{1/2}$$

$D_{H,0}$ is the diffusion coefficient for hydrogen and has a value of 6×10^{-5} m^2 s^{-1} and

$$D_{H,eff}^* = -0.0027 + 2.19 \times 10^{-6}\left(T_u - 273\right)$$

We use the value of d in conjunction with the information convective instabilities (described below) to calculate the thickness of lithosphere that has been rewetted and absorbed back into the conducting mantle.

2.7 Initial concentration of heat producing elements

^{40}K, ^{232}Th, ^{235}U, and ^{238}U provide the principle sources for radioactive heat in the Martian mantle. Estimates for the concentrations of these isotopes have come from studies of Earth's bulk composition and from meteorites believed to have been ejected from Mars [*Lodders and Fegley*, 1997; *Wänke and Dreibus*, 1994]. Table 1 provides a summary of the high and low

estimates for concentrations of heat-producing elements in Mars, as well as information about element's half-lives and associated heat productions.

Using this information, we can calculate the mean mantle heat production rate over time as [*Turcotte and Schubert*, 2002]

$$H = 0.9928 C_0^U H^{U\,238} \exp\left(\frac{t \ln 2}{\tau_{1/2}^{U\,238}}\right) + 0.0071 C_0^U H^{U\,235} \exp\left(\frac{t \ln 2}{\tau_{1/2}^{U\,235}}\right)$$

$$+ C_0^{Th} H^{Th} \exp\left(\frac{t \ln 2}{\tau_{1/2}^{Th}}\right) + 1.19 \times 10^{-4} C_0^K H^{K\,40} \exp\left(\frac{t \ln 2}{\tau_{1/2}^{K\,40}}\right)$$

<div align="right">Equation 75</div>

Figure 2 demonstrates the range of initial heat production in Mars due to the different estimates for elemental concentrations. Initial values for heat production in W range from 2.34×10^{-11} to 4.93×10^{-11}. This translates to initial heat source density values, Q_0, that range from 8.25×10^{-8} to 1.74×10^{-7} W/m^3. We investigate the effects of changing Q_0 in our thermal evolution models.

3.0 Results

3.1 Nominal Model

A nominal model provides a basis for comparison on which we can monitor the effects of varying initial conditions. The results from this model are similar to the results of *Hauck and Phillips* [2002]. The nominal model does not account for the viscosity contrast between wet and dry mantle, rewetting of depleted mantle lithosphere by diffusion of hydrogen, or compositional buoyancy. In order to best match predicted estimates of Martian crustal thicknesses [*McGovern et al.*, 2002; *Wieczorek and Zuber*, 2004; *Zuber et al.*, 2000; *Zuber*, 2001], we use the lower, near-chondritic heat production model of *Wänke and Dreibus* [1994]. The initial concentration of light elements in the core is also set to a moderate value of $x_0 = 0.2$. This condition has the

result that no inner core grows over the course of the model, which is in agreement with the lack of a Martian dynamo. A complete listing of all the initial conditions for this model is provided in Appendix II.

Figure 3 illustrates the results of the nominal model. Mantle temperature decreases monotonically over time, while Moho temperature initially increases as a result of the sequestration of heat producing elements in the crust. Over time, Moho temperature begins to decrease with the decay of these radioactive elements. Mantle melting and crust formation cease after ~0.7 Ga years and ~100km of crust has formed. The values for core and surface heat flux, as well as heat flux at the base of the crust, are similar to values reported by *Hauck and Phillips* [2002]. These values range from ~40 mW/m^2 at the beginning of the model's integration, to ~10 mW/m^2 at the end. There is no inner core formation.

The model predicts that the ratio between processed mantle to primitive mantle is ~ 2:1, indicating that the entire mantle has been melted almost twice over. The rapid mantle processing has caused a large amount of water and heat producing elements to be released from the solid-phase early in the planet's evolutionary history; only 20% of the initial concentration of water and heat producing elements remain at the end of mantle melting. The reasons for and consequences of this result are discussed further in the discussion section.

3.2 Effect of compositional buoyancy

Melted mantle is depleted in incompatible elements and less dense that unmelted mantle. In a stagnant lid system such as that on Mars, these density stratifications are expected to cause instabilities in the depleted mantle layer [*Parmentier and Hess*, 1992]. The change in density with respect to degree of melting (ϕ) may be expressed as [*Korenaga*, 2006]

$$\left(\frac{d\rho}{d\phi}\right) \approx -1.2 \text{ kg m}^{-3}/\%$$

We incorporate the effects of this compositional buoyancy into our thermal evolution model of Mars. We calculate the parameter $d\varrho$ in the heat-flow scaling law of *Korenaga* [Submitted] to be

$$d\rho = \frac{\rho_m - \phi_{avg}\dfrac{d\rho}{d\phi}}{\rho_m}$$

where ϕ_{avg} is the time averaged degree of melting.

The differences in the thermal evolution between the nominal model and the model incorporating compositional buoyancy are minimal. Slightly less crust (~1.5km) is produced when compositional buoyancy is turned on, and a slightly thicker (~5km) depleted lithosphere forms. More mantle is processed than in the nominal model as well, which leads a greater degree of dehydration, although the difference is only on the order of 0.5%. Overall, composition buoyancy does not play a significant role in the cooling of Mars.

3.3 Effect of dehydration stiffening

As previously mentioned, the dehydration of upwelling mantle will create viscosity contrasts between wet and dry mantle on the order of $10^2 - 10^3$ for dislocation creep scenarios [*Hirth and Kohlstedt*, 1996; *Korenaga and Karato*, 2008] and ~10 for diffusion creep [*Korenaga and Karato*, 2008]. Dehydration stiffening should occur in a step-like manner; i.e. viscosity will increase by a few orders of magnitude within a narrow depth interval [*Korenaga*, Submitted]. This effects of this step-like depth dependence has not been previously examined in terms of

thermal evolution, and it was predicted to create a stiff dehydrated lid that reduces surface heat flux [*Korenaga*, Submitted].

The results of using viscosity contrasts of 1, 10, and 100 under conditions with compositional buoyancy are shown in figure 4. The outcome of these models show that the influence of dehydration induced viscosity stratification has a noticeable effect on both thermal and crustal evolution. Higher viscosity contrasts results in higher final mantle temperatures and lower surface final temperature. Higher viscosity contrasts also result in significantly less crustal production; crust produced with viscosity contrast of 1 has a thickness ~100km while crust produced with a viscosity contrast of 100 has a final thickness of ~45km. Crust created under a higher viscosity contrast regime forms slower than crust formed in the nominal model. Additionally, crust formation begins at a later time and mantle convection ceases at a later time under higher viscosity contrast conditions.

Changing viscosity contrasts also affects values for surface and core heat flux early in the planet's evolution, with higher contrasts producing lower heat fluxes in accordance with the predictions of *Korenaga* (Submitted). Finally, a viscously stratified mantle is more quickly and efficiently dehydrated. The nominal model results in a mantle with only ~15% of it's initial water content remaining, while a high viscosity contrast results in a mantle with ~22% of it's original water content.

3.4 Effect of rewetting of depleted mantle lithosphere

We have examined the effects of rehydration by hydrogen diffusion into the depleted mantle lithosphere in the case with viscosity stratification. Rehydration of a depleted portion of the mantle had the potential to undermine the significance of the effects of viscosity stratification. We found, however, that the addition of a parameter to account for this

dehydration had little effect on the results of the thermal and crustal evolution model. All of the parameters remained relatively unchanged between the models with and without rehydration with the exception of crustal thickness. The model without rehydration generated a crustal thickness of ~45km while the model with rehydration resulted in a crust ~42km thick.

3.5 Effect of varying initial mantle temperature

Mantle temperature plays a key role in convection and melting in terrestrial planets. Initial mantle temperature has three main effects on the system [*Hauck and Phillips*, 2002]. First, a higher mantle temperature allows for a greater melt fraction, which in turn leads to the more rapid generation of crust. The convection velocity also increases with increasing mantle temperature, allowing for a greater amount of material to pass through the melt channel. This also has the effect of generating more crust. Finally, thermal temperatures influence the potential formation of an inner core. The formation of an inner core has the ability to create a magnetic field around Mars [*Stevenson*, 2003].

We examine the effects of varying the initial temperature of the upper mantle, T_{u0}, in order to fully appreciate the effects of thermal conditions in a viscosity and compositionally stratified mantle. Figure 5 illustrates the results when the model was run under conditions of T_{u0} = 1750K (nominal), 1850K, and 1950K. Almost 100km more crust was produced in the high initial temperature condition, consistent with the expectation that higher temperature would generate more crust more rapidly. High initial mantle temperatures also resulted in a larger percentage of processed (melted) mantle and a more complete dehydration of the mantle.

3.6 Effect of varying initial concentration of heat producing elements

Two main models predict radically different concentrations of radioactive heat producing elements in the Martian mantle [*Lodders and Fegley*, 1997; *Wänke and Dreibus*, 1994]. We

examine the effects of the predictions from both of these models, as well as the effects of an "average" heat production value, on thermal evolution with a viscously and compositionally stratified mantle. There are two main differences between the high and low heat generation models. First, more heat producing elements produces creates a greater melt fraction, which in turn generates more crust at a faster rate. Second, a mantle conforming to the *Lodders and Fegley* [1997] prediction of a greater amount of heat producing elements becomes almost completely dehydrated after ~1Ga. The model with a heat-producing elemental concentration predicted by *Wänke and Dreibus* [1994] retains ~22% of its original water content.

3.7 Effect of changing initial varying initial concentration of light constituents in the core

The variable x_0 represents the concentration of light constituents, such as sulfur, in the planetary core. This value is thought to range between 0.1 (sulfur-poor) and 0.25 (sulfur-rich). Lower values of x_0 results in earlier formation of an inner core [*Stevenson et al.*, 1983]. Inner core formation is significant because it can lead to compositional convection in the core, which in turn may create a magnetic field [*Stevenson*, 2003]. Mars currently has no measurable magnetic field, although a variety of evidence suggests that it may have had one in the past [*Acuna et al.*, 1998; *Connerney et al.*, 2001].

The only parameters that varying x_0 affects are core heat flux and inner core radius. Consistent with the results of *Stevenson et al.,* [1983], we find that lower initial concentrations of light elements in the core results in earlier inner core growth. With a value of $x_0 = 0.1$, the planet experiences inner core growth after ~2.5Ga. This beginning of inner core growth also causes an increase in core heat flux, although this increase does not affect any of the other observable parameters. Models run with core and mantle temperatures of 2200K and 1950K

respectively (nominal model has core and mantle temperatures with 2000K and 1750K) still result in inner core growth when $x_0 = 0.1$.

4.0 Discussion

4.1 Feasibility of model results

We can make an initial assessment of the feasibility of our new thermal evolution model by comparing the results of the model with independent predictions about the thickness and duration of emplacement of the Martian crust. Geophysical and geochemical studies have used physical evidence to place estimates on the thickness of the Martian crust. These studies employ a variety of geophysical and geochemical techniques that include analyses of Martian gravity and topography data, the moment of inertia of Mars, the viscous relaxation of topography, and geochemical mass balance calculations based on the composition of Martian meteorites and soils [*Wieczorek and Zuber*, 2004]. The underlying assumptions and precision with which each of the studies has been carried out vary, leading to a range of constraints on the thickness of Martian crust. On the whole however, these studies predict Martian crustal thickness values that lie between ~30 - ~115km, [*McGovern et al.*, 2002; *Nimmo and Stevenson*, 2001; *Wieczorek and Zuber*, 2004; *Zuber et al.*, 2000; *Zuber*, 2001]. When taking into consideration the effects of dehydration stiffening and compositional buoyancy, the model with $\Delta\eta = 100$ generates 42km of crust while the model with $\Delta\eta = 10$ produces ~68km of crust. These results are well within the feasible range for Martian crustal thickness estimates.

Previous papers have also been able to place constraints the rates of crustal growth. Using gravity and topography data, these studies have predicted that the large Tharsis volcanic

province was emplaced by the late Noachian to early Hesperian era[1] [*Hauck and Phillips*, 2002; *Phillips et al.*, 2001].   *Hauck and Phillips* [2002] state that the crust must have been stabilized by the time of Tharsis formation, and therefore a significant fraction of the crust must also have been emplaced by ~4Ga or earlier.   Model runs incorporating the effects of mantle melting also fit this constraint, particularly the model with $\Delta\eta = 10$.

4.2 Mantle melting effects

We were able to examine the role of viscosity and compositional stratifications on the complete thermal and crustal evolution of Mars. Incorporation of compositional buoyancy and rewetting of the deplete mantle lithosphere due to hydrogen diffusion had little, if any, effect of the results of our parameterized cooling model. Dehydration stiffening, however, does play a large role in determining the course of thermal evolution and crustal growth of Mars. Increasing the viscosity contrast between wet and dry mantle affects crustal and lithospheric thickness, heat flux values, and mantle and core temperatures.

The significance of dehydration stiffening on the thermal evolution of Mars is based on the assumption that Mars contained some amount of water in its primitive mantle; a completely dry mantle would clearly not experience the effects of dehydration. Estimates for the amount of water in the Martian mantle are based on studies of Martian meteorites and vary widely in their predictions. Studies of the Chassigny Martian meteorite yields potential water contents that range from 1ppm [*Mysen et al.*, 1998] to 1000 ppm [*Johnson et al.*, 1991].   The study of the Shergottite meteorite source magma have also yielded predictions of up to 1.8 wt% water in the Martian mantle [*McSween et al.*, 2001].   While the estimates of water content vary between

---

[1] The history of Mars is divided into three periods based on crater densities: Noachian (4.5-3.5 Ga), Hesperian (3.5 – 1.8 Ga), and Amazonian (1.8 Ga – present)

these studies, all indicate that the expectation of a wet Martian mantle is a reasonable assumption.

The importance of dehydration stiffening in thermal evolution is also dependent on the mineralogical composition of the Martian mantle. While water has been shown to have a strong influence on the viscosity behavior of olivine-dominated materials [*Korenaga and Karato*, 2008], it plays less of a role in determining the viscosity of pyroxene-dominated system. The amount of olivine in the mantle therefore greatly influences the amount of viscosity contrast between wet and dry mantle. The composition of Mars is poorly constrained due to the extremely limited number of available mantle source rocks. Previous papers have used compositions of Martian meteorites and models of the planet's density distribution with depth to make inferences about the bulk composition of planet's mantle [*Zuber*, 2001]. There are reports that the upper mantle of Mars consists primarily of olivine, similar to Earth [*Dreibus and Wanke*, 1985] and under this assumption, dehydration stiffening should occur and influence thermal evolution.

4.3 Dehydration and processing of the mantle

Our models suggest that the Martian mantle has lost between 70-90% of its original water due to dehydration. This estimate contradicts the prediction of only 10% water loss made by *Hauck and Phillips* [2002]. One reason for this discrepancy between the two studies may due to our smaller partition coefficient describing the degree of incompatibility of water. *Hauck and Phillips* [2002] used parameter D=0.1 for all of their models because they found minimal differences in crustal production for D=0.1 and D=0.01. They did not, however, investigate the effects the partition coefficient had on other aspects of the model, such as amount of dehydration. Their model may resemble our results with a smaller value for D.

The amount of processed mantle has never been studied before, and our models suggest that the amount of mantle melting throughout the planet's history is significant. The appropriate initial conditions can result in the entire Martian mantle being completely melted almost two-fold times. The large degree of melting in the mantle explains the high levels of dehydration, and plays an important role in the thermal evolution of the planet that cannot be overlooked.

4.4 Relationship between dehydration and crustal production

All of the model results indicate greater amounts dehydration of the mantle associated with the production of more crust. That this relationship exists despite the fact that models were run under a large variety of initial conditions suggests that the association between crust formation and dehydration is robust. Using studies on current crustal thickness estimates may allow us to infer information about the amount of water that was degassed from the dehydrating Martian mantle early in the planet's history.

Figure 6 plots the percentage of original water remaining in mantle versus crustal thickness, and each point represents the results of a model run with different initial conditions as indicated. The data form a linear trend that may be approximated with the relationship

$$\% \; H_2O \; remaining \; = \; -0.0012h_c + 0.2546$$

<div align="right">Equation 78</div>

If we assume an average crustal thickness of 50km [*McGovern et al.*, 2002; *Wieczorek and Zuber*, 2004], this relationship indicates that the mantle is ~80% dehydrated from its primitive state.

The mass of the Martian mantle is approximately

$$M_{mantle} = \frac{4}{3}\pi\left(R_p - R_c\right)^3 \cdot \rho_m = 5.2 \times 10^{23} \, kg$$

<div align="right">Equation 79</div>

Assuming an average water content of ~36ppm [*Dreibus and Wanke*, 1985], the total mass of water in the mantle is

$$M_{water} = M_{mantle} \cdot \frac{36}{10^6} = 2.1 \times 10^{19} \, kg$$

and the amount of degassed water is

$$M_{lost} = 0.8 \cdot M_{water} = 1.7 \times 10^{19} \, kg$$

which corresponds to a volume of 1.7×10^{16} m^3. The total surface area of Mars is

$$SA_{Mars} = 4\pi R_p^2 = 1.4 \times 10^{14} \, m^2$$

so this volume of water would create an global ocean ~117m deep.

Recent remote sensing studies have provided a wealth of mineralogical evidence to support that idea of a large body of liquid water on Mars that would have coincided with the period of mantle degassing. The Mars Exploration Rover *Opportunity* has discovered evidence of an ancient lakes [*Grotzinger et al.*, 2005], while the OMEGA spectrometer aboard *Mars Express* has detected numerous phyllosilicate minerals that were most likely formed during long periods of surface hydration [*Poulet et al.*, 2005]. Geophysical studies as well have provided evidence for water oceans on early Mars, and these studies have further hypothesized that the amount of water on early Mars would be equivalent to a global coverage of ~156m [*Carr and Head*, 2003], very similar to our predicted value of ~117m.

5.0 Summary

The thermal evolution of terrestrial bodies is a complex process that is influenced by many variables. We have shown that varying even one of these initial conditions or model parameters can have a large and sometimes unpredictable effect on the outcome of the model. Due to the complex, self-regulating nature of thermal evolution, the full effects of processes that influence cooling is best appreciated when studied using a self-consistent thermal evolution model.

We have created such a model that takes into account crustal and lithospheric growth. We found that dehydration stiffening caused by mantle melting plays an important role in the thermal evolution of Mars, while compositional buoyancy and rehydration of the depleted mantle lithosphere by hydrogen diffusion have a less influential impact. Our models also show a robust relationship between the amount of crust produced and water dehydrated from the planetary mantle. When used with estimates of modern day crustal thickness, this correlation allows us to predict that large amount of the mantle became dehydrated early in the planet's history. Water that was outgassed from the dehydrating mantle may have released enough water to cover the planet with a global ocean hundreds of meters deep.

6.0 Acknowledgements

7.0 References Cited

Acuna, M. H., et al. (1998), Magnetic field and plasma observations at Mars: Initial results of the Mars global surveyor mission, *Science*, *279*(5357), 1676-1680.

Carr, M. H., and J. W. Head (2003), Oceans on Mars: An assessment of the observational evidence and possible fate, *Journal of Geophysical Research-Planets*, *108*(E5), -.

Connerney, J. E. P., et al. (2001), The global magnetic field of Mars and implications for crustal evolution, *Geophysical Research Letters*, *28*(21), 4015-4018.

Dreibus, G., and H. Wanke (1985), Mars, a Volatile-Rich Planet, *Meteoritics*, *20*(2), 367-381.

Grotzinger, J. P., et al. (2005), Stratigraphy and sedimentology of a dry to wet eolian depositional system, Burns formation, Meridiani Planum, Mars, *Earth and Planetary Science Letters*, *240*(1), 11-72.

Hauck, S. A., and R. J. Phillips (2002), Thermal and crustal evolution of Mars, *Journal of Geophysical Research-Planets*, *107*(E7), -.

Hauri, E. H., et al. (1994), Experimental and Natural Partitioning of Th, U, Pb and Other Trace-Elements between Garnet, Clinopyroxene and Basaltic Melts, *Chemical Geology*, *117*(1-4), 149-166.

Hirth, G., and D. L. Kohlstedt (1996), Water in the oceanic upper mantle: Implications for rheology, melt extraction and the evolution of the lithosphere, *Earth and Planetary Science Letters*, *144*(1-2), 93-108.

Johnson, M. C., et al. (1991), Chassigny Petrogenesis - Melt Compositions, Intensive Parameters, and Water Contents of Martian (Questionable) Magmas, *Geochimica Et Cosmochimica Acta*, *55*(1), 349-366.

Koga, K., et al. (2003), Hydrogen concentration analyses using SIMS and FTIR: Comparison and calibration for nominally anhydrous minerals, *Geochemistry Geophysics Geosystems*, *4*, -.

Korenaga, J. (2006), Archean geodynamics and the thermal evolution of earth, *Archean Geodynamics and Environments*, *164*, 7-320.

Korenaga, J., and S. I. Karato (2008), A new analysis of experimental data on olivine rheology, *Journal of Geophysical Research-Solid Earth*, *113*(B2), -.

Korenaga, J. (Submitted), Scaling of stagnant-lid convection with Arrhenius rheology and the effects of mantle melting.

Lachenbruch, A. H. (1970), Crustal Temperature and Heat Production - Implications of Linear Heat-Flow Relation, *Journal of Geophysical Research*, *75*(17), 3291-&.

Lodders, K., and B. Fegley (1997), An oxygen isotope model for the composition of Mars, *Icarus*, *126*(2), 373-394.

Lunine, J. I., et al. (2003), The origin of water on Mars, *Icarus*, *165*(1), 1-8.

McGovern, P. J., et al. (2002), Localized gravity/topography admittance and correlation spectra on Mars: Implications for regional and global evolution, *Journal of Geophysical Research-Planets*, *107*(E12), -.

McSween, H. Y., et al. (2001), Geochemical evidence for magmatic water within Mars from pyroxenes in the Shergotty meteorite, *Nature*, *409*(6819), 487-490.

Mysen, B. O., et al. (1998), The role of H_2O in Martian magmatic systems, *American Mineralogist*, *83*(9-10), 942-946.

Nimmo, F., and D. J. Stevenson (2001), Estimates of Martian crustal thickness from viscous relaxation of topography, *Journal of Geophysical Research-Planets*, *106*(E3), 5085-5098.

Parmentier, E. M., and P. C. Hess (1992), Chemical Differentiation of a Convecting Planetary Interior - Consequences for a One Plate Planet Such as Venus, *Geophysical Research Letters*, *19*(20), 2015-2018.

Phillips, R. J., et al. (2001), Ancient geodynamics and global-scale hydrology on Mars, *Science*, *291*(5513), 2587-2591.

Poulet, F., et al. (2005), Phyllosilicates on Mars and implications for early martian climate, *Nature*, *438*(7068), 623-627.

Reese, C. C., et al. (1998), Heat transport efficiency for stagnant lid convection with dislocation viscosity: Application to Mars and Venus, *Journal of Geophysical Research-Planets*, *103*(E6), 13643-13657.

Solomatov, V. S., and L. N. Moresi (2000), Scaling of time-dependent stagnant lid convection: Application to small-scale convection on Earth and other terrestrial planets, *Journal of Geophysical Research-Solid Earth*, *105*(B9), 21795-21817.

Stevenson, D. J., et al. (1983), Magnetism and Thermal Evolution of the Terrestrial Planets, *Icarus*, *54*(3), 466-489.

Stevenson, D. J. (2003), Planetary magnetic fields, *Earth and Planetary Science Letters*, *208*(1-2), 1-11.

Takahashi, E., and I. Kushiro (1983), Melting of a Dry Peridotite at High-Pressures and Basalt Magma Genesis, *American Mineralogist*, *68*(9-10), 859-879.

Turcotte, D., and G. Schubert (2002), *Geodynamics*, 2nd ed., Cambridge University Press.

Wanke, H., and G. Dreibus (1994), Chemistry and Accretion History of Mars, *Philosophical Transactions of the Royal Society of London Series a-Mathematical Physical and Engineering Sciences*, *349*(1690), 285-293.

Wieczorek, M. A., and M. T. Zuber (2004), Thickness of the Martian crust: Improved constraints from geoid-to-topography ratios, *Journal of Geophysical Research-Planets*, *109*(E1), -.

Zuber, M. T., et al. (2000), Internal structure and early thermal evolution of Mars from Mars Global Surveyor topography and gravity, *Science*, *287*(5459), 1788-1793.

Zuber, M. T. (2001), The crust and mantle of Mars, *Nature*, *412*(6843), 220-227.

Appendix 1: Tables & Figures
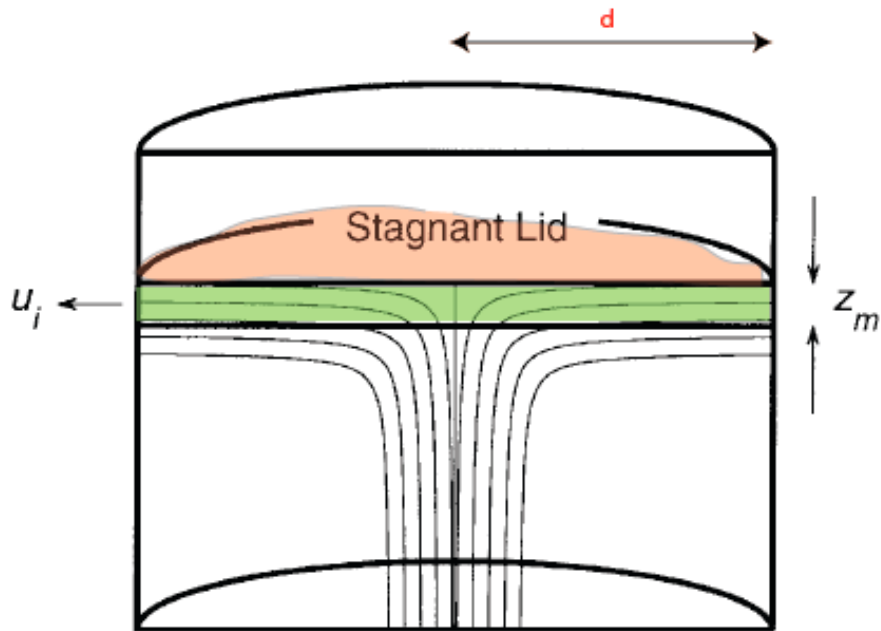
Figure 1: *(From Reese et al., 1998)* Schematic illustration of mantle melting cylinder. Melting begins at the depth z_m and u_i demonstrates the convective velocity of the melt.

Isotope	% Total	High Mars Value	Low Mars Value	H (W kg^{-1})	$\tau_{1/2}$ (years)
^{238}U	99.28%	15.88 ppb	15.88 ppb	9.46×10^{-5}	4.47×10^9
^{235}U	0.71%	0.11 ppb	0.11 ppb	5.69×10^{-4}	7.04×10^8
^{232}Th	100%	55 ppb	56 ppb	2.64×10^{-5}	1.40×10^{10}
^{40}K	0.0119%	920ppm	305ppm	2.92×10^{-5}	1.25×10^9

Table 1: Abundances and half-lives of most common heat producing elements. High Mars values are from *Lodders and Fegley* [1997] and low Mars values are from *Wänke and Dreibus* [1994].
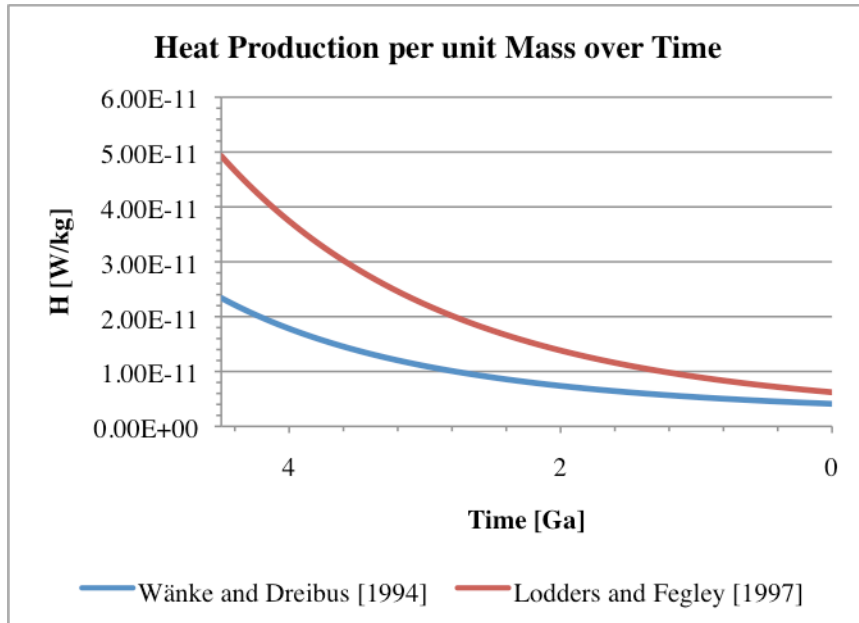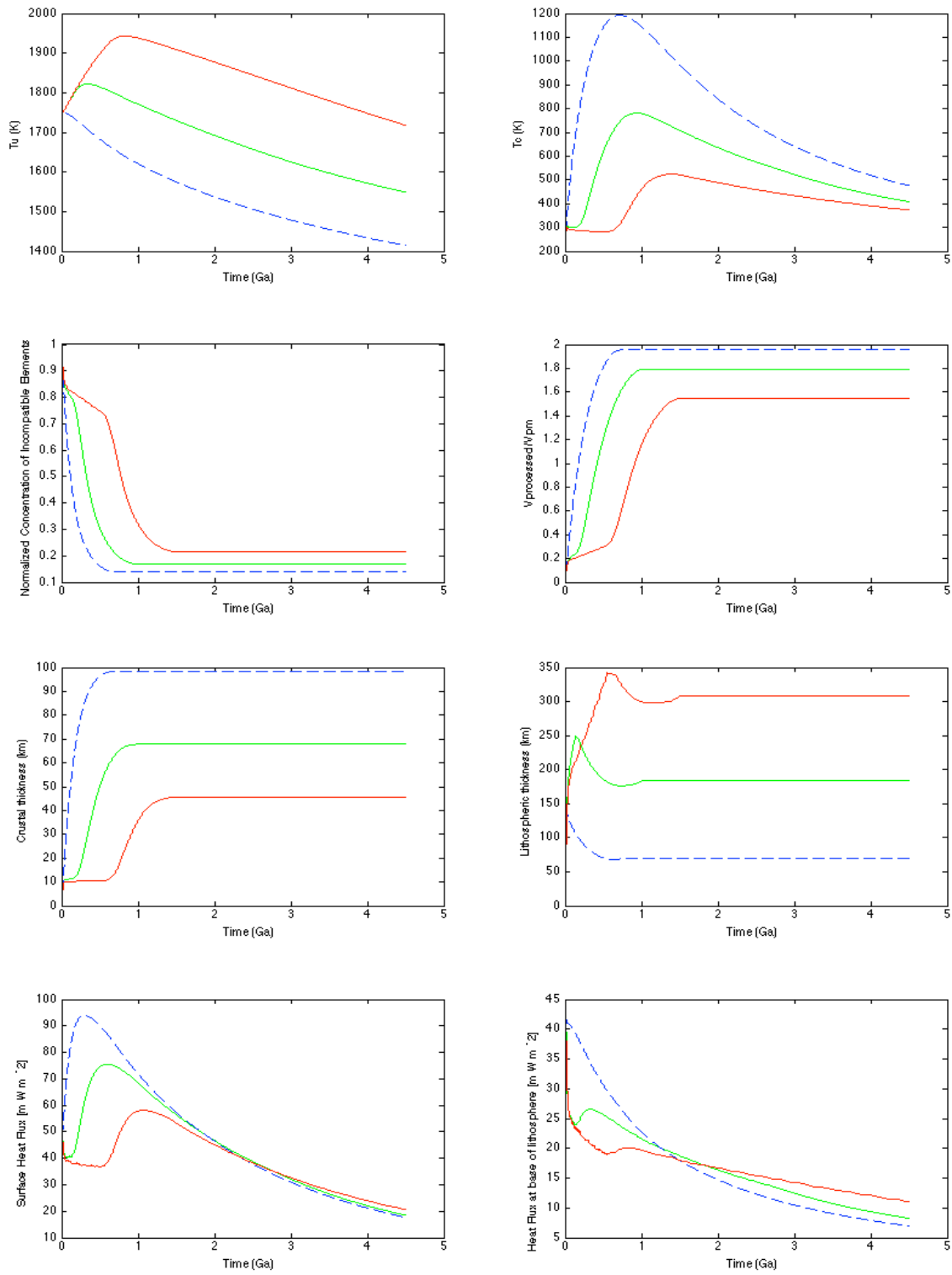
**Figure 2:** Heat production per unit mass as a function of time.
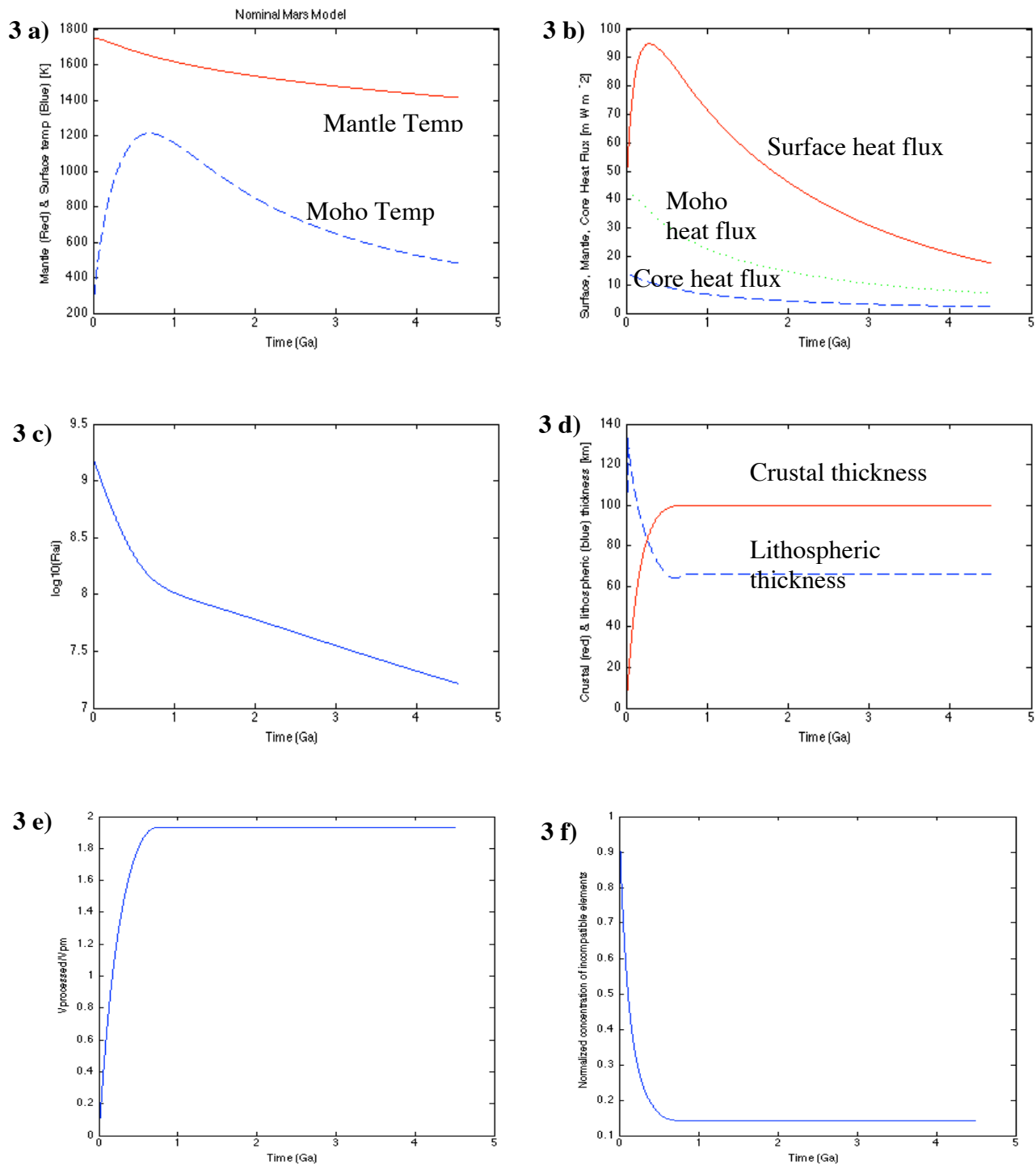
Figure 3: Key results from the nominal Mars model. (**a**) Mantle (red) and Moho (blue) temperature (**b**) Surface (red), Moho (green), and core (blue) heat flux (**c**) Rai (**d**) Crust (red) and lithospheric (blue) thickness (**e**) Ratio of processed to primitive mantle (**f**) Normalized concentration of incompatible elements remaining

Figure 4: Key results from runs with viscosity contrasts. Δη =1 shown in blue, Δη =10 shown in green, Δη =100 shown in red.
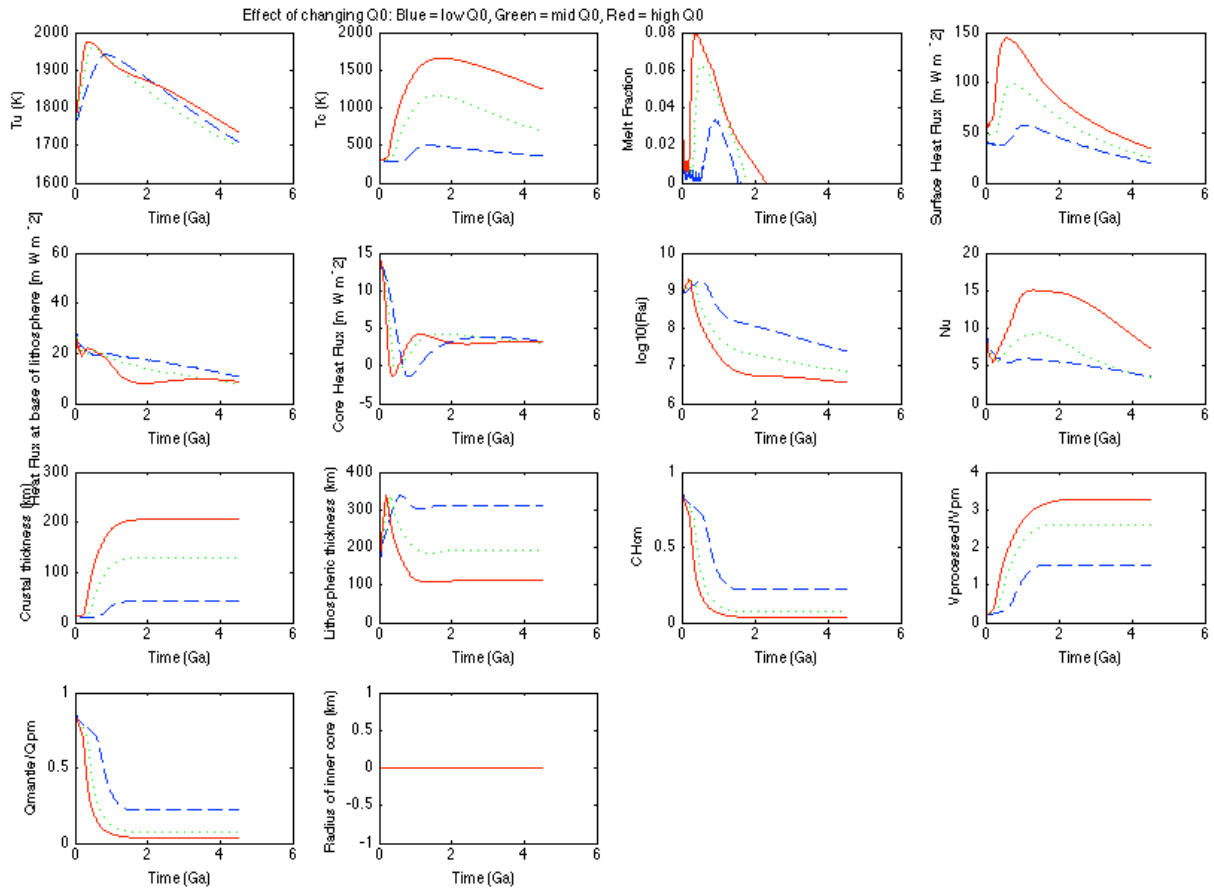
Figure 5: Full results from varying initial potential temperatures. Red: $Q_0 = 1.74 \times 10^{-7}$, Green: $Q_0 = 1.24 \times 10^{-7}$, Blue: $Q_0 = 8.25 \times 10^{-8}$
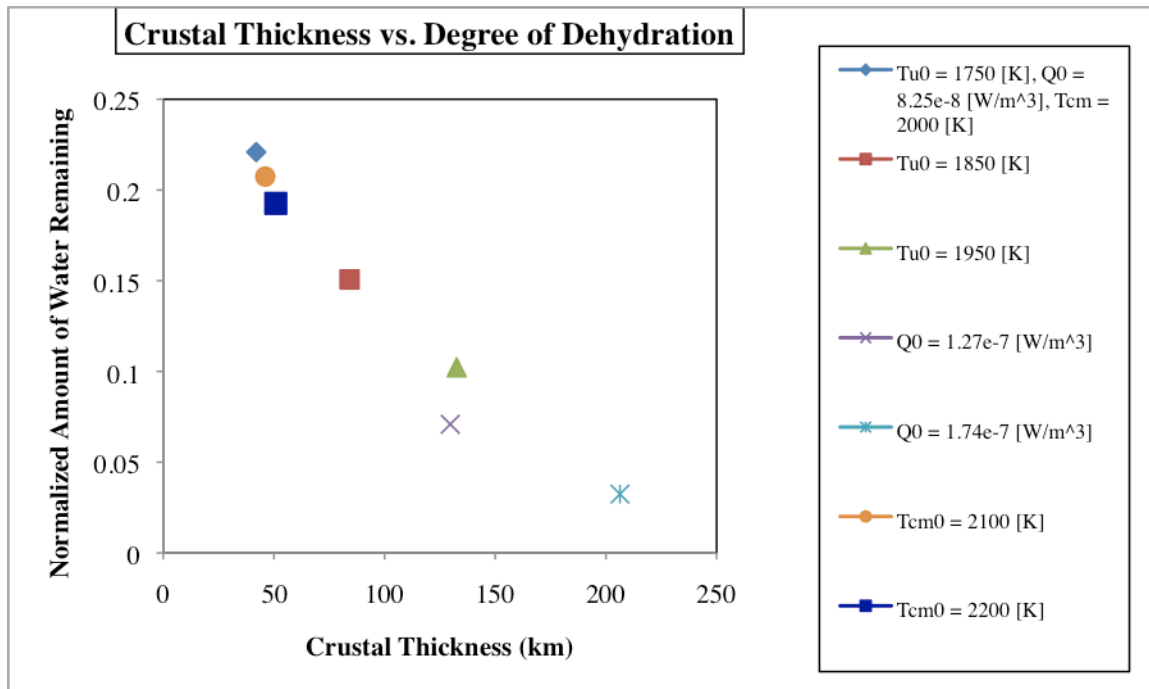
Figure 6: Relationships between crustal thickness and degree of dehydration. Nominal model in this graph incorporates effects of mantle melting and has T_{u0} = 1750K, Q_0 = 8.25e-8, T_{cm0} = 2000K

Appendix II: Parameter Variables in Nominal Model

Model parameters:

Name	Value	Description
α_c	2	Constant
α	2×10^{-5}	Volumetric coefficient of thermal expansion [K]
k	4.0	Constant, [W m^{-1} K^{-1}]
K	10^{-6}	Average thermal diffusivity of the mantle in [m^2 sec^{-1}]
λ	1.38×10^{-17}	Average density constant [s]
A	5.2×10^{4}	Constant [K]
ν_0	4.0×10^{3}	Constant [m^2 s^{-1}]
Ra_{Cr}	5.0×10^{2}	Critical Rayleigh number for the onset of convection
B	0.3	Constant
Ra_{Crb}	2×10^{3}	Rayleigh number for critical breakdown of thermal boundary layer
g	3.7	Gravitational constant [m s^{-2}]
T_s	220	Surface temperature [K]
T_{m1}	13.6×10^{-12}	Constant [K Pa^{-1}]
T_{m2}	-62.2×10^{-24}	Constant [K Pa^{-3}]
T_{a1}	8.00×10^{-12}	Constant [K Pa^{-1}]
T_{a2}	-39×10^{-24}	Constant [K Pa^{-3}]
η_m	1.00	Constant
η_c	1.10	Constant
T_{m0}	1809	Iron melting temperature [K]
L_{pm}	600×10^{3}	Mantle latent heat of melting [J/K]
R_p	3390000	Planet radius [m]
R_c	1550000	Core radius [m]
ϱ_m	3527	Density of mantle [kg m^{-3}]
C_m	1149	Heat capacity of mantle [J kg^{-1} K^{-1}]
ϱ_c	7200	Density of core [kg m^{-3}]
C_c	571	Heat capacity of core [kg m^{3}]
μ	80×10^{9}	Rigidity [Pa]
m	2.5	Grain size exponent
E	240×10^{3}	Activation energy [J mol^{-1}]
R	8.314	Gas constant [J K^{-1} mol^{-1}]
P_c	40.0×10^{9}	Pressure at the planet's center [Pa]
P_{cm}	19.0×10^{9}	Pressure at the core-mantle boundary [Pa]
$L+E_g$	5×10^{5}	Latent heat of solidification and gravitational energy made available per unit mass of inner core [J kg^{-1}]
n	1	Stress exponent

Initial conditions:

Name	Value	Description
x_0	0.2	Initial concentration of light constituents in the core
T_{u0}	1750	Initial value of T_u [K]
T_{cm0}	2000	Initial value of T_{cm} [K]
R_{i0}	0	Initial value of inner core radius [m]
Q_0	8.25	Initial heat source density [W m^{-3}]
$\Delta\eta$	1	Viscosity contrast between wet and dry mantle
$d\varrho/d\Phi$	0	Compositional buoyancy